Experimental Comparison of the Wake of a Vertical Axis Wind Turbine and Planar Actuator Surfaces

Huang, M.; Ferreira, C.; Sciacchitano, A.; Scarano, F.

DOI
10.1088/1742-6596/1618/5/052063

Publication date
2020

Document Version
Final published version

Published in
Journal of Physics: Conference Series

Experimental Comparison of the Wake of a Vertical Axis Wind Turbine and Planar Actuator Surfaces

Experimental Comparison of the Wake of a Vertical Axis Wind Turbine and Planar Actuator Surfaces

M Huang, C Ferreira, A Sciacchitano and F Scarano

AWEP Department, Faculty of Aerospace Engineering, Delft University of Technology, Kluyverweg 1, 2629 HS Delft, The Netherlands.

Email: M.Huang-1@tudelft.nl

Abstract. Wind tunnel experiments on a scaled vertical axis wind turbine (VAWT) and square porous plate with a porosity of 64% are conducted in the W-tunnel of TU-Delft. The VAWT thrusts in axial and lateral directions are measured with an in-house load cell system based on moment conservation. Wake of the VAWT in tip speed ratio of 1.5 and 2.5 and the porous plate is measured with the robotic particle image velocimetry technique, which enables a three-dimensional velocity measurement in a combined volume encompassing from 1 diameter upstream to 3 diameters downstream. Counter-rotating vortex pairs in VAWT wake and the wake shape deformation and deflection are discussed, which are related to the lateral thrust. A square porous plate inducing a similar axial thrust is compared, which has the same shape as the cross-section of the VAWT. Wake of the right porous plate with a yaw angle of 15° is investigated, which produces similar deflection as the VAWT.

1. Introduction

Simplified VAWT models inducing similar wakes are important to study the wake effect in a VAWT farm because they enable more rapid aerodynamic analysis. Specifically, they enable fast estimates of the velocity deficit, turbulence intensity, and wake shape. And it can be practical to experimentally study large VAWT arrays with simplified models. To make reasonable simplifications, the nature of VAWT wakes needs to be studied. However, confined to the differences in turbine configuration and operating conditions, previous VAWT wake studies may not show consistent properties, for instance, the structure of the wake that is much related to the solidity and tip speed ratio (TSR, λ) of a specific turbine [1,2]. Thus, consistent property accounting for both TSR and solidity needs to be found out and quantified. An alternative property is the thrust coefficient, C_T, which is one of the most important parameters for the actuator disc theory. The actuator disc theory is widely used in kinematic wake models for horizontal axis wind turbines (HAWT) [3–5], simplified models for HAWTs based on this theory has been experimentally studied and validated extensively [6–9].

In contrast, there are only a few experimental studies on simplified VAWT models. Craig *et al*. (2017) [10] conducted PIV measurements in the wake of rotating cylinders and rectangular meshes with different porosity to investigate the applicability of low order physical models for VAWTs. They concluded that the actuator square may produce similar far wake when VAWTs rotate in low TSR range (from 1 to 2). Moreover, experiments conducted at Re = 600 imply laminar or transitional development of the boundary layer along the blade, differing from the regime encountered on wind turbines. Besides, the thrust coefficient is not quantified in their work. Thus, there are still questions about whether a planar actuator can work as a simplified surrogate for a VAWT, and what is the mechanism back or against such simplifications.

In this work, experiments are conducted that compare the three-dimensional flow development in the wake of a scaled two-blade VAWT and a planar plate with a porosity of 64%, to examine the feasibility of representing a VAWT with a planar actuator. Loads are measured with 4 load cells mounted on the support structure, and the velocity field from 1 diameter upstream up to 3 diameters downstream of the VAWT and the plate are measured using robotic particle image velocimetry (robotic PIV [11]). The velocity and vorticity fields are compared among the different models.

Low TSRs (less than 2.5 in this case) are needed to avoid high streamwise thrust coefficient, which can easily exceed 1.0 because of the high solidity of the VAWT. Moreover, it is challenging for actuator disc based model to predict the wake of heavily loaded wind turbines [12]. Thus, to make a fair comparison, TSRs of 1.5 and 2.5 are chosen, which are similar to that of the previous studies by Craig *et al*. (2017) [10].

2. Experimental setup

Experiments are conducted at the W-tunnel of the TU Delft Aerodynamic Laboratories, The W-tunnel is an open-jet wind tunnel with a square 0.6 m × 0.6 m exit. The wake is measured using robotic PIV. The robotic PIV system consists of three major parts: the coaxial volumetric velocimeter (CVV), comprised of a compact arrangement of four CMOS cameras (10 bits, 704 × 464 pixels) at low tomographic aperture and an optical fiber delivering the light emitted by a Nd:YLF Quantronix Darwin Duo Laser (21 mJ pulse energy @ 1 kHz, 527 nm wavelength), a robotic arm (Universal Robots UR5) that allows the robotic manipulation of the CVV system with six degrees of freedom, and the helium-filled soap bubbles (HFSB) seeding generator, which delivers sub-millimeter neutrally buoyant tracer particles. Figure 1 shows the overall experimental setup.

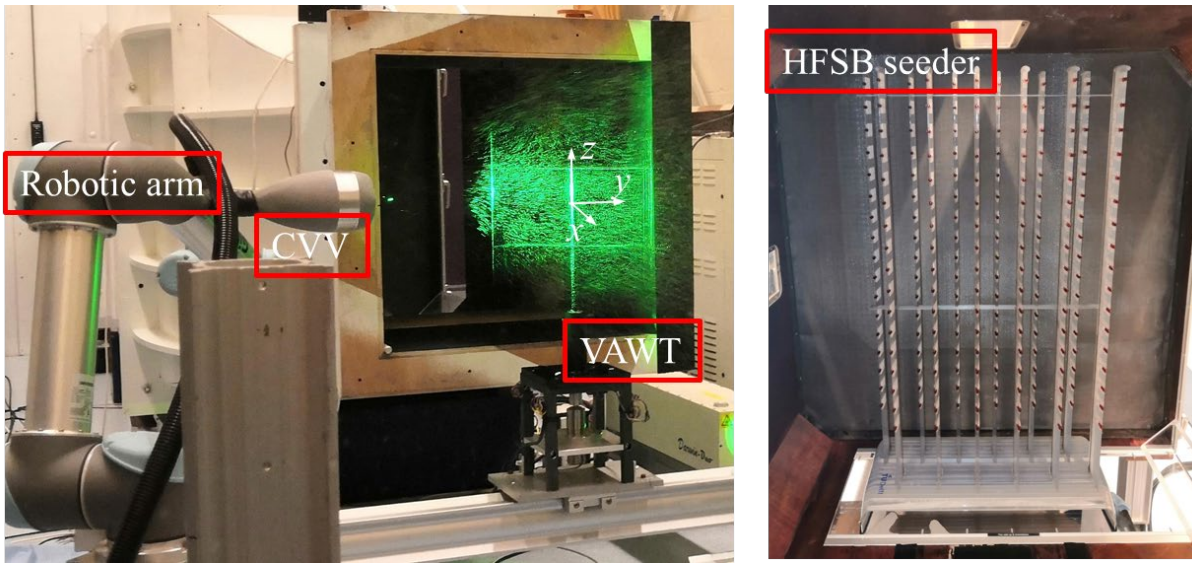

Figure 1. Experimental set up: Robotic PIV measuring (left), HFSB seeder inside the settling chamber of W-tunnel (right).

2.1. Scaled VAWT model and the load measurement system

The scales of the VAWT model and the schematic plotting of the load measurement system are shown in the left of Figure 2. The VAWT model has two blades, with a profile of NACA0012. The length of the blade is 300 mm, and the rotor diameter is 300 mm. The model is driven by a DC motor, to reach a tip speed ratio (TSR) within the region of 1 – 5. The detailed design specifications are listed in Table 1.

Loads are measured with 4 load cells integrating with the supporting structure, which is at the base of the rotor, as shown in Figure 2. The wind flows towards *x*-direction, and forces acting on the center of the rotor are calculated based on moment balance [13]:

$$F_x = \left[\left(f_3 + f_4\right) - \left(f_1 + f_2\right)\right] \cdot \frac{d}{2h} \tag{1}$$

$$F_y = \left[\left(f_2 + f_3\right) - \left(f_1 + f_4\right)\right] \cdot \frac{d}{2h} \tag{2}$$

where d is the distance between the adjacent load cells, h is the distance between the rotor center and the installation plane of the load cells. In this work, d = 50 mm, h = 318 mm.

Table 1. VAWT design specifications

Property	Dimension
Number of Blades	2
Blade length	300 mm
Rotor diameter	300 mm
Blade profile	NACA0012
Chord blade	3 mm
Strut profile	NACA0012
Chord strut	3 mm

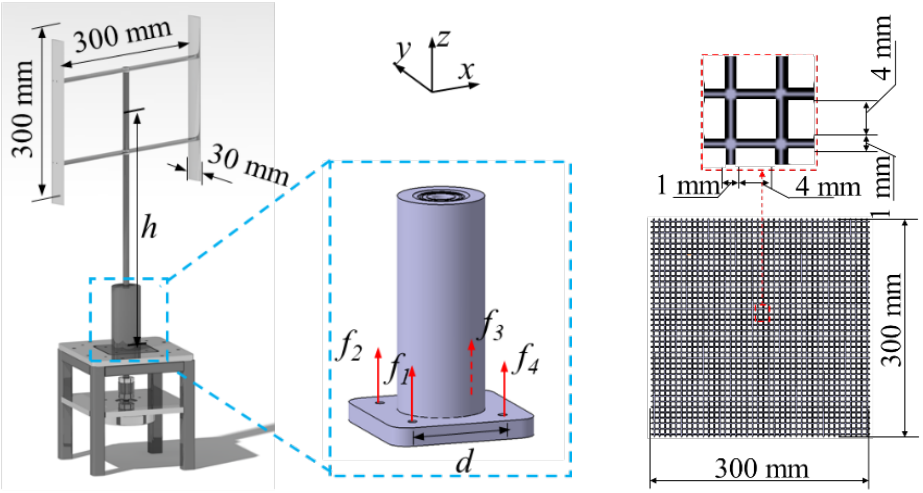

Figure 2. Schematic plotting of the models: VAWT model with a thrust measurement system (left) and porous plates (right).

2.2. Porous plates

The porous plate is 3D printed. The aperture of the plate is 4 mm, the pitch is 5 mm, resulting in a porosity of 64%, as shown in Figure 2. The thickness is 2 mm. The geometry details are listed in Table 2. To make a fair comparison with the VAWT model, the mesh was mounted on the same strut as the VAWT during the measurement.

Table 2. Porous plate geometry specifications

Property	Plate A
Size	300 × 300 × 2 mm^3
Porosity	64%
Aperture	4 mm
Pitch	5 mm

2.3. Measurements and data processing procedure

The total measurement volume is obtained combining the individual measurements from different positions of the robotic PIV system. Figure 3 shows the measurement views in the horizontal (*X-Y*) and vertical (*Y-Z*) plane, respectively. In the present study, 48 positions for the instantaneous field of view (IFOV) are chosen. At each position, 5000 images are recorded at a rate of 804 images per second (measurement time of 6.3 s). The motion of the CVV system by the robotic arm is controlled using the RobotDK software. Image acquisition and storage requires approximately half a minute for each measurement position.

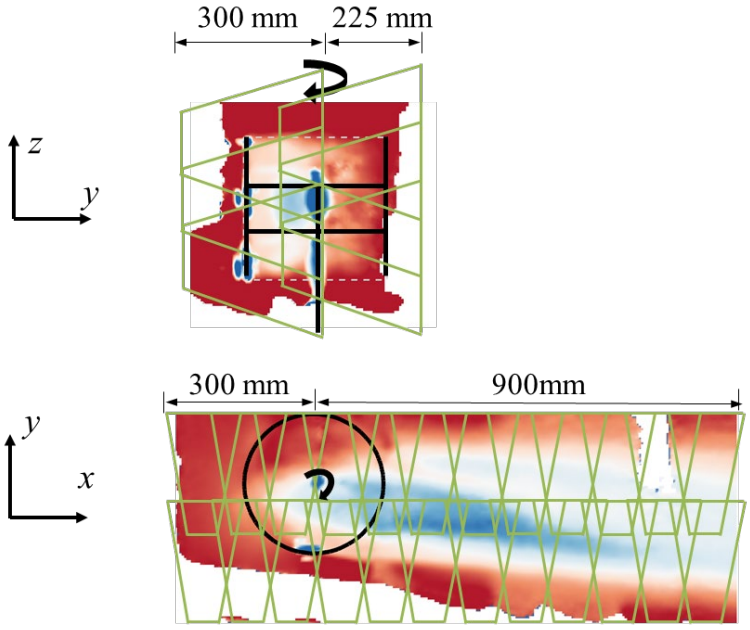

Figure 3. Measurement views in the horizontal (X-Y) and vertical (Y-Z) plane.

3. Results

3.1. Thrust coefficient comparison

The time-averaged forces applied on the center of the rotor are measured with varying the tip speed ratio (TSR, λ), thus the streamwise and lateral forces produced by the VAWT model are:

$$T_x = -F_x;\ T_y = -F_y \tag{3}$$

where the negative signs mean the thrusts are opposite to the positive direction of the x and y-axis, respectively.

Thrust coefficients are calculated as:

$$C_T = \frac{T}{0.5\rho A V^2} \tag{4}$$

where ρ is the air density, A is the projected rotor area, V is the inflow velocity. The time-averaged force coefficients applied to the flow by the VAWT are depicted in Figure 4. The streamwise thrust coefficients, $C_{T,x}$, and the overall thrust coefficients, C_T increase as the tip speed ratio increasing. In contrast, the lateral thrust, $C_{T,y}$, decreases at higher tip speed ratios. As comparison, the thrust coefficients versus yaw angle for porous plate is plotted in figure 5. From yaw angle from 0 to 5 degrees, $C_{T,x}$ increases due to a higher projected porosity in streamwise. However, projected disc area in streamwise is decreasing meanwhile, which causes decrease of $C_{T,x}$ from 5 to 10 degrees. In contrast, $C_{T,y}$ and C_T increase as larger yaw angle.

Figure 6 presents C_T induced by porous plates versus the porosity, measured data without yaw angle in this work (marked as 'This work') is compared with data documented in the literature.

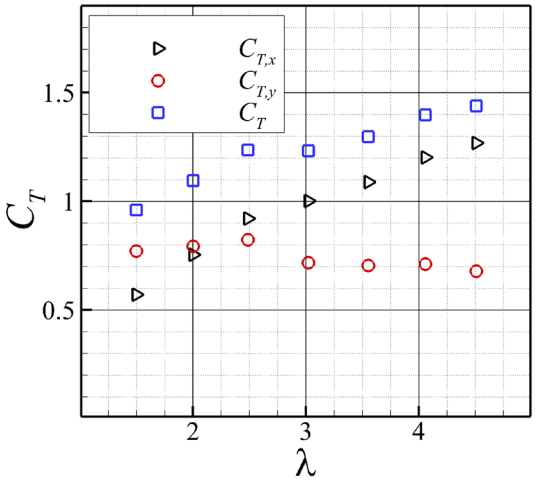

Figure 4. The time-averaged streamwise, lateral and overall thrust coefficients of the VAWT, $C_{T,x}$, $C_{T,y}$, and C_T, vary with tip speed ratio, λ.

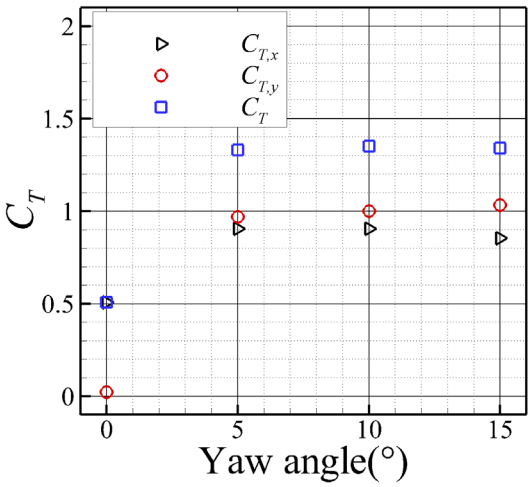

Figure 5. The time-averaged streamwise, lateral and overall thrust coefficients of porous plates vary with yaw angle.

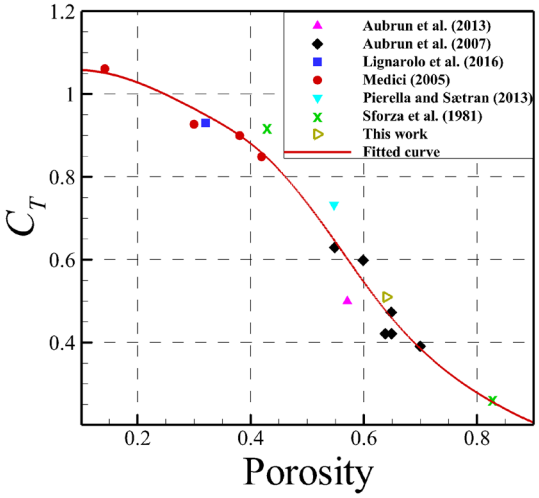

Figure 6. Thrust coefficient of porous plates as a function of porosity in literature.

3.2. VAWT and planar actuator wake comparison

In this section, the wakes of the VAWT in TSR 1.5 and 2.5 along with the porous plate wake with and without yaw are presented. As aforementioned, these working regimes can avoid heavily loaded condition, and similar ones are adopted in previous work in terms of wake study [2][10]. It should be noted that dynamic stall happens in these regimes, as investigated for instance by Buchner *et al* (2018) [14] and Ferreira *et al* (2009) [15]. Moreover, the high lateral forces presented in this work could partly be ascribed to dynamic stall.

3.2.1. Counter-rotating vortex pairs in the VAWT wake. The velocity fields on *Y-Z* planes along axial positions are shown in figure 7 and 8, where the velocity developments under λ = 1.5 and λ = 2.5 are presented respectively. Solid frame with ticks denotes the projected area of the wind tunnel nuzzle, and dashed square is the projected outline of the VAWT swept area. The VAWT in higher TSR suffers a deeper stream-wise velocity deficit due to a higher axial thrust coefficient, and this is consistent with the thrust measurement result in Figure 4.

Counter-rotating vertex pairs (CVPs) are observed, resulting in an asymmetric wake shape, as well as a deflection towards the windward region. When λ = 1.5, the induced force on the advancing blade is considerably higher than the retreating blade, as a result, the maximum deficit and CVP locates at the windward region. This CVP induces a side flow, deflecting the wake towards the windward side. Moreover, the CVP stretches the wake shape into an asymmetric shape, where more vertical expansion presents on the windward side.

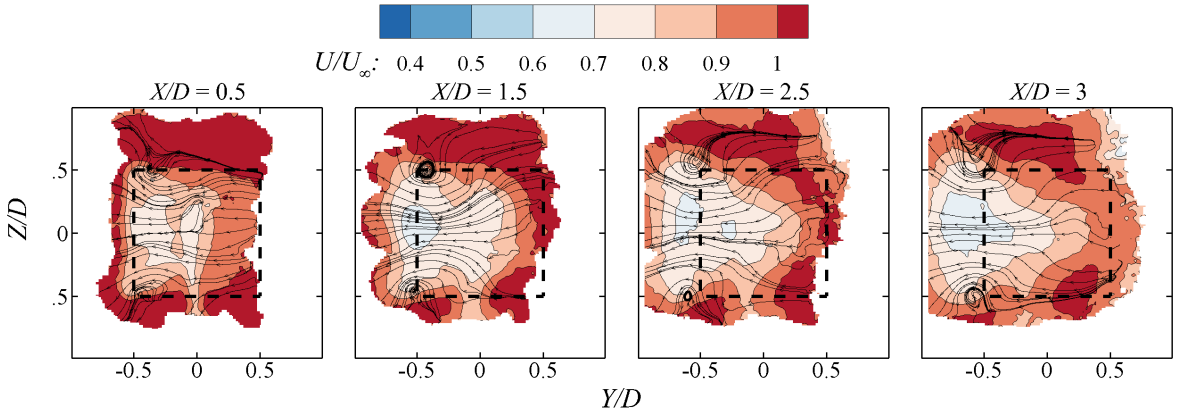

Figure 7. Stream-wise velocity contours and in-plane sreamlines at cross-sections downstream of the VAWT rotating in TSR of 1.5 (*X/D* = [0.5, 1.5, 2.5, 3]).

The wake in higher TSR shows features alike to that of lower TSR, in particular the side-flow and the asymmetric wake shape. When the VAWT rotates with λ = 2.5, the effect of the retreating blade becomes stronger, thus the induced CVP locates less towards the windward position compares to VAWT wake under λ = 1.5. This could explain why the deflection seems a bit less under higher TSR.

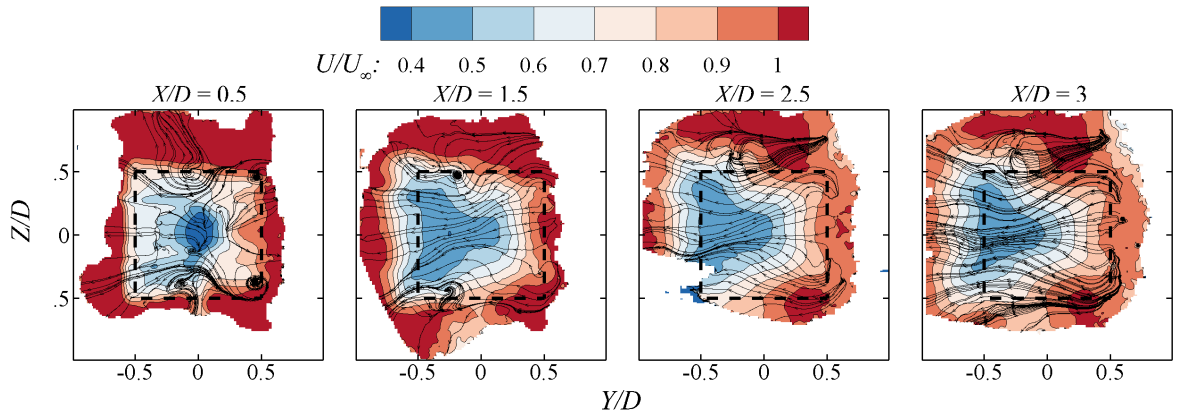

Figure 8. Stream-wise velocity contours and in-plane streamlines at cross-sections downstream of the VAWT rotating in TSR of 2.5 (*X/D* = [0.5, 1.5, 2.5, 3]).

Similar CVP are reported by Rolin and Porté-Agel [2], they investigated the wake recovery mechanism of a VAWT model, and concluded that CVP accounts for most of the energy entrainment,

and it is related to the lateral force. Ryan *et al* [16] also reported this phenomenon, and it was ascribed to the tip vortices in their work. In fact, the measured lateral forces under these TSRs are almost constant as discussed, which is consistent with the wake deflection and deficit shown by the velocity fields in Figure 7 and Figure 8. These pieces of evidence confirm that the vortex pairs are related to the lateral force. It should be noted that lateral force is caused by the asymmetric force distribution along the blade swept path.

3.2.2. Wake shape and vorticity system in the planar actuator wake. The normalized streamwise velocity contours and in-plane velocity vectors at X/D = 1.5 are depicted in Figure 9. We observe a symmetric wake shape which is different from that of a VAWT. Inward flows around the corners are driven by CVPs, making the wake into a clover-leaf shape. This CVP distribution is due to the planar actuator shape effect, in comparison with that of a VAWT, which is caused by the asymmetric lateral force distribution. And the forces of a VAWT results in a variation in crossflow momentum [2]. In contrast, less lateral momentum entrainment happens in the wake of a planar actuator disc, and this could be the reason why the actuator disc wake suffers more deficit in the near wake when the induced axial force is similar. Some outward flows at the edges are observed, that is because 1.5 diameter downstream is still in the near wake region, where wake expansion is still pronounced.

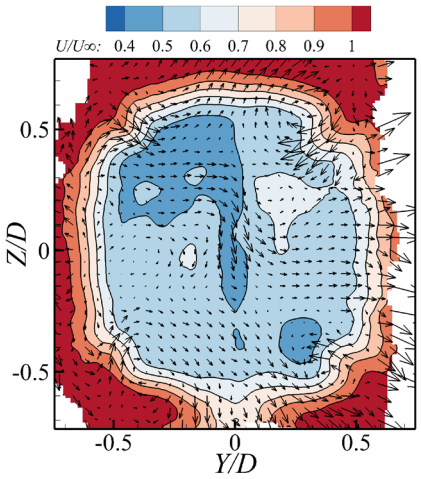

Figure 9. Stream-wise velocity contour and in-plane velocity vectors of the plate perpendicular to the flow (X/D = 1.5)

Craig et al. [10] used a yawed rectangular porous mesh producing lateral induction to mimic VAWT wake, and they concluded that a static actuator can produce a quite similar wake with VAWTs in low TSR (from 1 to 2). To examine the idea of representing a VAWT with a planar actuator disc, the velocity contours of the yawed actuator disc are studied. Figure 10 shows the cross-sectional stream-wise velocity contour and in-plane velocity vectors at X/D = 1.5, the yellow contour line denotes where the velocity is zero. Compared with the wake of VAWT and porous plate without yaw, the wake of yawed plate suffers a higher velocity deficit, even reverse flow is imparted inside the yellow contour line. The expansion is stronger as well, which implies a higher axial thrust induced. This is because of the equivalent porous is decreased when yawing the mesh, and lower porosity leads to higher thrust with other conditions kept the same.

The outline of the wake cross-section seems like a tilted cloverleaf, in relation with the wake of a square actuator that is perpendicular to the inflow. This tilted shape is mostly caused by a strong cross-flow, that results from a pair of pronounced vortices generated around the wake center. Thus, asymmetric development is presented.

The center of the wake at X/D = 1.5 is around Y/D = -0.25, similar to that of VAWT in λ = 1.5 and 2.5. This phenomenon implies that the deflection of the porous plate is comparable with the VAWT.

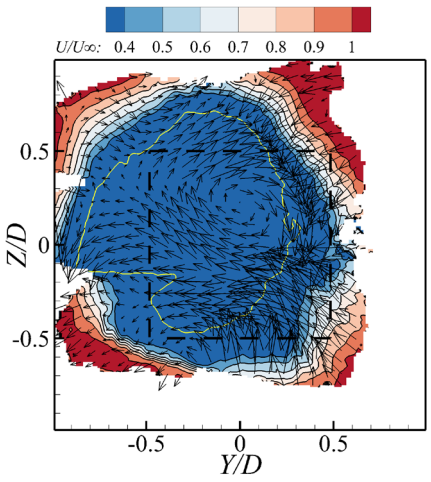

Figure 10. Stream-wise velocity contour and in-plane velocity vectors of the plate in yaw, the yellow line denoted the zero velocity. (X/D = 1.5, yaw angle = 15°)

3.2.3. Deflection and expansion in the VAWT wake. To compared the wake deflection and expansion, velocity fields over the *XY* plane crossing rotor center are shown from figure 11 to 13. The blue contour line denotes where the velocity attains to 90% of inflow velocity. According to the streamlines and the contour lines, it is clear that the wake is deflected towards the windward region, and the deflection angles for TSR of 1.5 and 2.5 are close. This is because of the CVPs and lateral forces discussed in section 3.2.1. are in a similar strength. In the leeward side, the wake develops nearly align with the freestream. On the other hand, wake in $\lambda = 2.5$ features a similar pattern except for a larger deficit.

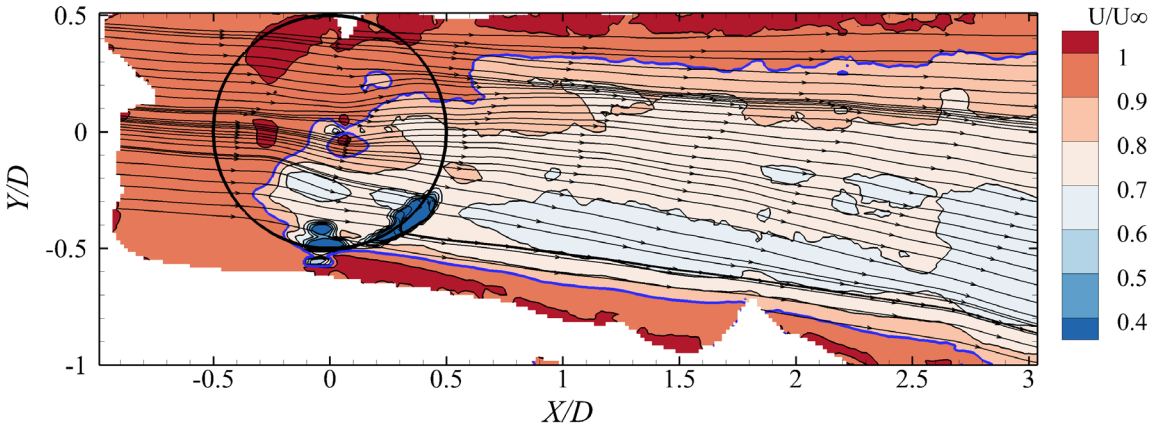

Figure 11. Time-averaged and normalized stream-wise velocity contour and streamlines in the *XY*-plane along with the streamline, $Z/D = 0$, $\lambda = 1.5$.

3.2.4. Wake deflection by yawing the actuator disc.

Figure 13 shows the velocity contour and streamlines of the yawed plate at $Z/D = 0$. A mask is implemented around the plate position, where a large error was caused by reflection. The yellow line shows where the velocities equal to zero. A pronounced vortex is imparted on one side of the recirculation region, pushing the wake to the other side. The entire wake is deflected even though the expansion is strong. It should be noted that to match a similar velocity deficit and wake deflection is a bit tricky because yawing a mesh will change the equivalent porosity. And the cross-sectional shape of the wake of VAWT and porous plate features large differences, which could also make a planar actuator surface a poor representative of a VAWT.

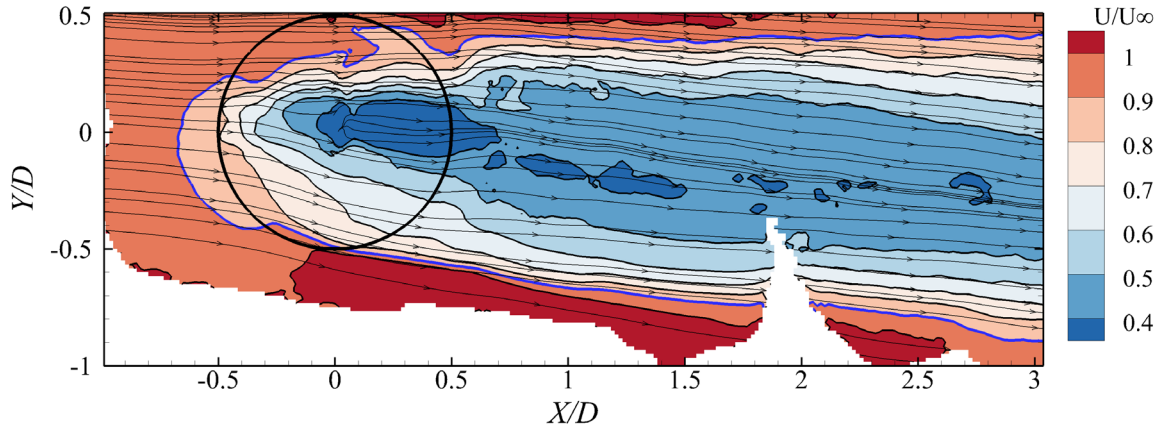

Figure 12. Time-averaged and normalized stream-wise velocity contour and streamlines in the *XY*-plane along with the streamline, $Z/D = 0$, $\lambda = 2.5$.

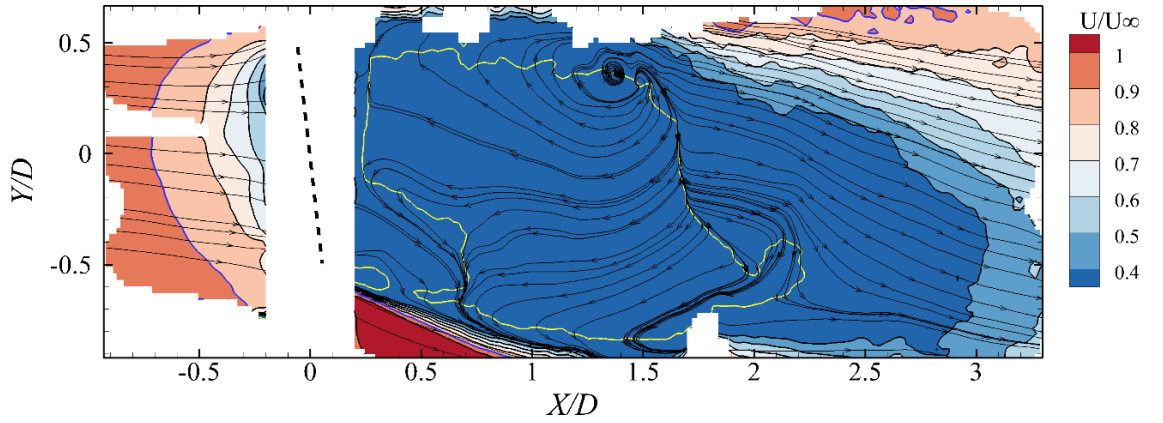

Figure 13. Time-averaged and normalized stream-wise velocity contour and streamlines in the XZ-plane at Y/D = 0.

4. Conclusions

In this present study, the thrust coefficient and averaged streamwise velocity field of a scaled VAWT under $\lambda = 1.5$ and $\lambda = 2.5$ are studied, and a planar actuator with and without yaw is examined as a simplified surrogate of VAWT. Main conclusions can be made as follows:

1) Axial thrust of the VAWT model in this work increases as TSR goes higher, on the other hand, lateral thrust keeps nearly constant in lower λ (1 – 2.5), but decreases with higher λ (2.5 – 4.5).
2) CVPs found in the VAWT wake is related to the lateral force, which induces an asymmetric wake shape and deflection.
3) The VAWT wake is deflected towards the windward side. On the leeward side, the wake expansion compensates the deflection, and the streamline is almost aligned with the inflow.
4) Square porous plate cannot induce similar wake as a VAWT even with the same frontal area and a similar streamwise thrust coefficient. Large discrepancies are observed in terms of the cross-sectional shape and velocity deficit, even in the far wake region.
5) Planar actuator disc inducing a similar streamwise thrust with a VAWT can cause a higher deficit in the wake. CVPs present around the corners, and no lateral forces are induced when the porous plate is not yawed.
6) Yawed actuator disc presents a stronger velocity deficit and expansion in the wake, implying a higher induced streamwise thrust.

Acknowledgements
The present research is partly supported by the China Scholarship Council, grant number: CSC No. 201806290006.

References

[1] Tescione G, Ragni D, He C, Simão Ferreira C J and van Bussel G J W 2014 Near wake flow analysis of a vertical axis wind turbine by stereoscopic particle image velocimetry *Renew. Energy* **70** 47–61
[2] Rolin V F C and Porté-Agel F 2018 Experimental investigation of vertical-axis wind-turbine wakes in boundary layer flow *Renew. Energy* **118** 1–13
[3] Jensen N O 1983 A note on wind generator interaction *Risø-M* **2411**
[4] Larsen G C 1988 A Simple Wake Calculation Procedure *Risø-M* **No. 2760** 58
[5] Bastankhah M and Porté-Agel F 2014 A new analytical model for wind-turbine wakes *Renew. Energy* **70** 116–23
[6] Aubrun S, Loyer S, Hancock P E and Hayden P 2013 Wind turbine wake properties: Comparison between a non-rotating simplified wind turbine model and a rotating model *J. Wind Eng. Ind. Aerodyn.* **120** 1–8
[7] Aubrun S, Bastankhah M, Cal R B, Conan B, Hearst R J, Hoek D, Hölling M, Huang M, Hur C, Karlsen B, Neunaber I, Obligado M, Peinke J, Percin M, Saetran L, Schito P, Schliffke B, Sims-Williams D, Uzol O, Vinnes M K and Zasso A 2019 Round-robin tests of porous disc models *J. Phys. Conf. Ser.* **1256** 012004
[8] Howland M F, Bossuyt J, Martínez-Tossas L A, Meyers J and Meneveau C 2016 Wake structure in actuator disk models of wind turbines in yaw under uniform inflow conditions *J. Renew. Sustain. Energy* **8** 043301
[9] Yu W, Ferreira C and van Kuik G A M 2019 The dynamic wake of an actuator disc undergoing transient load: A numerical and experimental study *Renew. Energy* **132** 1402–14
[10] Craig A E, Dabiri J O and Koseff J R 2017 Low order physical models of vertical axis wind turbines *J. Renew. Sustain. Energy* **9** 1–17
[11] Schneiders J F G, Scarano F, Jux C and Sciacchitano A 2018 Coaxial volumetric velocimetry *Meas. Sci. Technol.* **29** 065201
[12] Schmitz S and Maniaci D C 2017 Methodology to determine a tip-loss factor for highly loaded wind turbines *AIAA Journal* vol 55 pp 341–51
[13] Leblanc B P and Ferreira C S 2018 Experimental Determination of Thrust Loading of a 2-Bladed Vertical Axis Wind Turbine *J. Phys. Conf. Ser.* **1037** 022043
[14] Buchner A-J, Soria J, Honnery D and Smits A J 2020 Dynamic stall in vertical axis wind turbines: scaling and topological considerations *J. Fluid Mech* **841** 746–66
[15] Simão Ferreira C, Van Kuik G, Van Bussel G and Scarano F 2009 Visualization by PIV of dynamic stall on a vertical axis wind turbine *Exp. Fluids* **46** 97–108
[16] Ryan K J, Coletti F, Elkins C J, Dabiri J O and Eaton J K 2016 Three-dimensional flow field around and downstream of a subscale model rotating vertical axis wind turbine *Exp. Fluids* **57** 38